Available online at www.sciencedirect.com
ScienceDirect
Journal of Power Sources 176 (2008) 191–199
JOURNAL OF POWER SOURCES
www.elsevier.com/locate/jpowsour

A design tool for predicting the capillary transport characteristics of fuel cell diffusion media using an artificial neural network

E.C. Kumbur, K.V. Sharp, M.M. Mench *

Fuel Cell Dynamics and Diagnostics Laboratory, Department of Mechanical and Nuclear Engineering, The Pennsylvania State University, University Park, PA 16802, United States

Received 21 July 2007; received in revised form 16 October 2007; accepted 17 October 2007
Available online 25 October 2007

Abstract

Developing a robust, intelligent design tool for multivariate optimization of multi-phase transport in fuel cell diffusion media (DM) is of utmost importance to develop advanced DM materials. This study explores the development of a DM design algorithm based on artificial neural network (ANN) that can be used as a powerful tool for predicting the capillary transport characteristics of fuel cell DM. Direct measurements of drainage capillary pressure–saturation curves of the differently engineered DMs (5, 10 and 20 wt.% PTFE) were performed at room temperature under three compressions (0, 0.6 and 1.4 MPa) [E.C. Kumbur, K.V. Sharp, M.M. Mench, J. Electrochem. Soc. 154(12) (2007) B1295–B1304; E.C. Kumbur, K.V. Sharp, M.M. Mench, J. Electrochem. Soc. 154(12) (2007) B1305–B1314; E.C. Kumbur, K.V. Sharp, M.M. Mench, J. Electrochem. Soc. 154(12) (2007) B1315–B1324]. The generated benchmark data were utilized to systematically train a three-layered ANN framework that processes the feed-forward error back propagation methodology. The designed ANN successfully predicts the measured capillary pressures within an average uncertainty of ±5.1% of the measured data, confirming that the present ANN model can be used as a design tool within the range of tested parameters. The ANN simulations reveal that tailoring the DM with high PTFE loading and applying high compression pressure lead to a higher capillary pressure, therefore promoting the liquid water transport within the pores of the DM. Any increase in hydrophobicity of the DM is found to amplify the compression effect, thus yielding a higher capillary pressure for the same saturation level and compression.

Keywords: Artificial neural network; Capillary pressure; Gas diffusion layer; Polymer electrolyte fuel cell; Two-phase transport; Water management

1. Introduction

Proper selection of the fuel cell diffusion media (DM) design criteria is critical to achieve high fuel cell performance and durability, since the porous DM plays a deterministic role in establishing an effective micro-fluidic management in fuel cell operations [1–5]. To date, fuel cell manufacturers have invested considerable resources towards developing advanced DM materials with favorable internal architectures that will assist in resolving the water management issue. However, these efforts generally rely on trial-and-error approaches and require extensive testing programs due to the lack of benchmark data required to precisely couple the capillary transport processes with the internal structure of the porous DM.

The fuel cell DM is typically made of carbon–fiber-based products, such as non-woven carbon paper and woven cloth that have a non-uniform pore distribution. Because of the hydrophilic nature of these randomly packed carbon fibers, the DM substrates are impregnated with an anisotropic coating of PTFE, thereby yielding mixed wettability characteristics with bi-modal configuration [6–10]. The liquid water transport within the pores of the DM is mainly governed by capillary action, and phase change; hence in pore-level modeling studies, the DM is commonly modeled as a bundle of tortuous capillary tubes with variable radius [11,12]. In the capillary transport mode, the driving force is created by the local capillary pressure gradient, which is a strong function of water saturation, pore wettability and pore size [13]. Any change in pore morphology due to the possible change in PTFE content or fuel cell assembly compression will directly affect the local capillary pressure, thus resulting in a different water distribution [7,14–17]. Therefore, probing the change in the capillary pressure as a function of cell

* Corresponding author. Tel.: +1 814 865 0060; fax: +1 814 863 4848.
E-mail address: mmm124@psu.edu (M.M. Mench).

0378-7753/$ – see front matter © 2007 Elsevier B.V. All rights reserved.
doi:10.1016/j.jpowsour.2007.10.059

compression and PTFE loading of the DM is critical in terms of precisely quantifying the liquid water inside the DM.

Due to the inherent structural complexity of the DM and the apparent experimental limitations, most DM characterization studies rely on modeling efforts that are limited by the dubious correlations adopted from soil science. More importantly, these mathematically complex models serve to provide qualitative connection between the cell performance and the transport process. An excellent review of the recent modeling efforts is provided by Djilali [18]. However, in terms of design and optimization, the essential goal should be to provide a reliable tool that can precisely correlate the governing input–output relationship of the system. One way to achieve such a tool is to construct a non-parametric framework trained by actual benchmark data. To date, the increasing demand of such a design tool for PEFC materials has motivated the use of various approaches to achieve this goal. The artificial neural network (ANN) approach has emerged as a strong candidate, since it offers an alternative way to tackle complex and ill-defined problems with its excellent multi-dimensional mapping capability [19]. Recently, a few ANN studies [20–26] focused on prediction of the fuel cell performance based on experimental data or model simulations have been reported, however to the best of authors' knowledge, no direct study focused on predicting the capillary transport behavior of the fuel cell DM using ANN has been performed.

In terms of methodology, ANN systems simulate small individual interconnected adaptive units called neurons, which are inspired from biological neurons. These artificial neurons are designed to learn the system behavior based on external or internal information, which is fed through the network [27]. The network is composed of interconnected layers in which the clusters of artificial neurons carry information. Learning occurs through a training process where the relations between each layer are correlated and adjusted based on the supplied stream of information [28]. The unique feature of these trained networks is to accurately correlate the complex interrelated parameters of the system simply by ignoring the excess data that are of minimal significance [19]. This feature eliminates the need for detailed information about the system, thus enabling the network to handle large and complex systems. More detailed explanation of ANN systems is provided in Refs. [19,27,28].

This study addresses the development of a DM design tool using artificial neural network and newly available direct benchmark data [6–8] to describe the capillary pressure–saturation relationship in various fuel cell DMs. Direct drainage capillary pressure–saturation data have been generated for SGL 24 series DMs coated with different PTFE loadings (5, 10 and 20 wt.%) under three different compression loadings (0, 0.6 and 1.4 MPa). The detailed descriptions of our experimental approach and major findings have been documented in a series of publications [6–8]. The benchmark data compiled from these experiments have been integrated into the three-layered ANN that processes the feed-forward error back propagation methodology. The network was systematically trained with the novel benchmark data, and then utilized to delineate the relative significance of PTFE content and compression on the capillary pressure of this class of DM materials, within the range of tested parameters.

2. Method of approach

2.1. Experimental approach and data description

SGL 24 series (SIGRACET® gas diffusion layers) carbon paper DMs, namely SGL 24BC (5% PTFE), SGL 24CC (10% PTFE) and SGL 24DC (20% PTFE) were utilized in the benchmarking experiments [6–8]. The tested DM samples are treated with PTFE (hydrophobic agent) from 5 to 20 wt.% of total, which is in a typical hydrophobic treatment range preferred in conventional fuel cell applications. The base macro-porous substrate of the tested carbon paper DM samples is coated with a 50 μm thin micro-porous layer (MPL) of carbon black mixed with PTFE. In terms of hydrophobicity of the MPL, it was found in Ref. [6] and by Gostick et al. [29] that the micro-porous layer contains considerably fewer hydrophilic pores; therefore it is almost exclusively hydrophobic in nature. However, the exact value of the PTFE treatment during the processing of this thin micro-porous layer has not been publicly disclosed by the manufacturer. The material properties of the tested composite DM samples, as supplied by the manufacturer, are provided in Table 1.

To date, different techniques [4,30,31] have been used for measurement of the capillary saturation behavior of the fuel cell DM. Lin and Nguyen [4] measured the capillary pressure–saturation using a volume displacement method, whereas Acosta et al. [30] determined the imbibition and drainage curves via a mercury intrusion technique. Recently, Fairweather et al. [31] has reported a micro-fluidic device specially designed to measure the capillary pressure–saturation curves of the fuel cell DM during liquid and gas intrusion. In this study, a new technique, the method of standard porosimetry (MSP), was employed to measure the desired transport parameters such as capillary pressure, saturation, pore size, and

Table 1
Material properties of the tested DM samples

Material	Type	Thickness (μm)	PTFE (wt.%) (macro-substrate)	Porosity	Permeability ($cm^3\ cm^{-2}\ s^{-1}$)
SGL 24BC	Paper w/MPL	235	5	0.76	0.60
SGL 24CC	Paper w/MPL	235	10	0.75	0.60
SGL 24DC	Paper w/MPL	235	20	0.75	0.45

All values are adapted from manufacturer technical specification sheets. The same types of DMs (*i.e.*, SGL 24 Series) have been utilized in benchmarking experiments in order to eliminate any possible uncertainties associated with the fabrication processes of these materials. Note that the values of porosity, permeability, and PTFE content given in Table 1 represent the material properties of the tested macro-fuel cell diffusion media substrate (*i.e.*, macro-DM without MPL).

hydrophobic and hydrophilic porosity distribution. The use of this technique to measure the desired capillary transport properties of the fuel cell DM has been also reported by Gostick et al. [29]. The MSP is a reliable and established technique used for acquiring the necessary data regarding the capillary pressure–saturation behavior of porous materials [32]. This technique is based on a capillary equilibrium process and developed by Porotech Ltd. In these experiments, the DM samples were placed in capillary contact between two standard samples having a known capillary pressure–saturation curve [32]. At each equilibrium the corresponding capillary pressure and saturation values of the tested DM samples were measured based on the known capillary pressure–saturation characteristics of the standard samples [32]. Different liquids (de-ionized water and octane) were utilized as working fluids to evaluate the mixed wettability characteristics of DMs samples over a set of different compressions and PTFE loadings.

When MSP technique is compared with the traditional mercury intrusion porosimetry (MIP), mercury intrusion porosimetry is limited in that it is incapable of distinguishing the hydrophobic and hydrophilic pore distribution (dual pore network), and requires high pressures which can lead to a substantial deformation of the porous fuel cell DM structure [32]. These limitations are directly eliminated with the use of MSP. Since the MSP technique is based on the natural capillary equilibrium concept, the measurement with this technique does not require any external pressure. In addition, MSP enables precise measurements over a large range of pore sizes of different materials including soft or frail materials under different compression and temperatures [32]. A detailed description of this technique and the measured specific morphological characteristics for the tested DM samples are provided in Ref. [32] and [6–8], respectively.

The benchmarking experiments were performed for the DM samples given in Table 1 under different levels of compression loadings, *i.e.*, 0, 0.6 and 1.4 MPa to capture the corresponding changes in the pore configuration and the transport properties of the tested DM samples (*i.e.*, capillary pressure, saturation, porosity, bi-modal pore distribution and pore size). The measured capillary pressure data were compiled in a database and then categorized corresponding to the measured saturation, PTFE content of the DM and the operating compression. While MSP can not fully characterize the imbibition/drainage cycling (hysteresis effect) which the fuel cell DM could be exposed to under dynamic conditions, this technique is capable of measuring the drainage capillary pressure–saturation curves of the tested fuel cell DM samples. The capillary drainage flow characteristics of the hydrophobic pore network captured by the MSP technique are considered essential, since the hydrophobic pores form the flow pathways (conduits) for the liquid water to diffuse through the DM.

2.2. Neural network design and training

A feed-forward error back propagation neural network has been constructed for this study. The architecture of ANN consists of a three-layered network equipped with the tangent-sigmoid and log-sigmoid activation functions in hidden layers and a linear transfer function in the output layer to capture the highly non-linear relationship between the input and output parameters. The optimum number of neurons in the hidden layers has been determined based on a trial-and-error approach. A total number of 30 neurons, 10 neurons in each layer, have been found to be most suitable neuron configuration for the present ANN pattern. The input layer has been configured to include four correlated input parameters based on the non-wetting phase saturation, the compression pressure and the PTFE content of the DM, whereas the output layer is designed for one parameter, "the capillary pressure", which is a governing parameter for the capillary transport mechanism in DM. Note that the effects of relative and intrinsic permeability are also important for fully describing the capillary transport within the porous fuel cell DM, but are beyond the scope of this study. As noted previously, when the capillary-induced transport in fuel cell DM is analyzed, the driving force is created by the local capillary pressure gradient, which is a strong function of water saturation, pore wettability (PTFE effect) and pore size (compression effect). Therefore, in this study, the main focus is placed on predicting the capillary pressure as a function of these specified parameters (*i.e.*, saturation, PTFE content and fuel cell compression pressure). The method of approach and the schematic of the proposed network structure are presented in Fig. 1.

The connections between the sub-layers of the present neural network are represented by the weights or so-called synaptic connections, which are calibrated by feeding the network with a suitable set of training data. This supervised training mode allows the network to modify the connection weights and learn the intricate representation of the specified input parameters with respect to the desired outputs [27]. In the present feed-forward ANN model, the information supplied by the input parameters flows through the forward direction from input nodes to the output node, while the transferred information is systematically adjusted by the assigned weights. For each input-data set, the associated error has been calculated and then back propagated through the network layers to continuously update the weights. After performing sufficient cycle of supervised training, the network has achieved the ability to identify the appropriate input–output connections and an optimum match with the output data has been obtained.

2.3. Network validation

A total of 340 data sets were utilized in the training and testing phase of the present ANN model. Among these data set, 290 data sets were randomly chosen and implemented as a training set, while the remaining 50 data sets were utilized as a test set for cross-validation to improve the learning process. During the supervised training process, the associated learning error rate (mean-squared error) was minimized by increasing the number of training epochs (cycles). However, an optimal number of training epochs need to be determined in order to avoid any possible overtraining of the network. A total number of 3750 epochs were determined to be the optimum number of training cycles for the present ANN structure and the corresponding

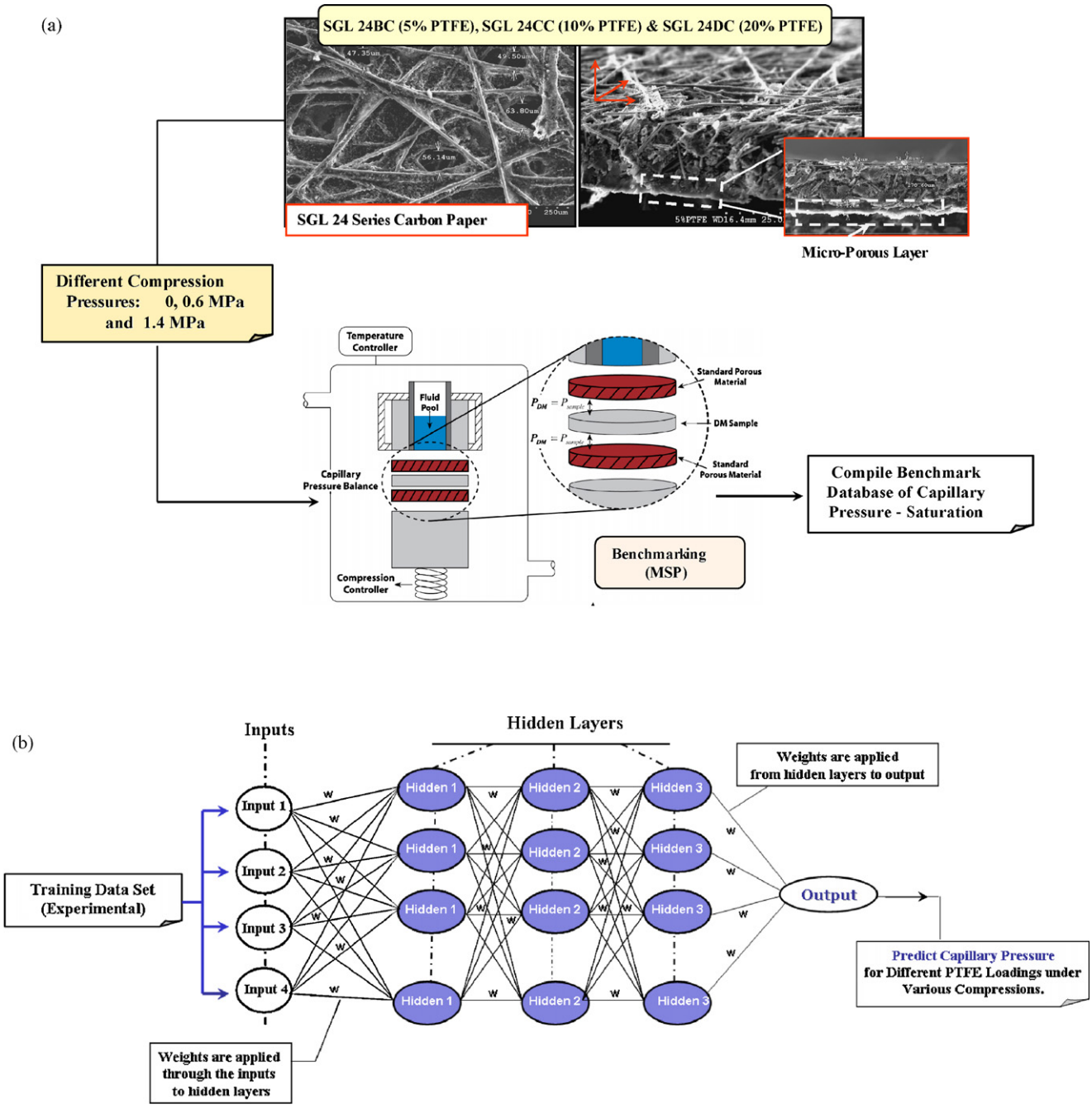

Fig. 1. (a) Method of approach including: MSP experiments, testing conditions, and tested DM samples [6–8] and (b) the schematic of the feed-forward neural network architecture designed for this study.

mean-squared error (relative error between the network output and target value) was found to be 3.4×10^{-8} at the end of 3750 training epochs. Fig. 2 shows the training epoch cycles versus the calculated mean squared error of the supervised training and the comparison of input benchmark data and corresponding ANN predictions for the training process. After the best learning performance was obtained with the specified training scheme, a detailed comparison of the experimental data with the ANN predictions based on discrete input data set (different than the data set used in training process) was performed for the tested DM samples to evaluate the prediction quality of the designed neural network.

Fig. 3a shows the measured and ANN prediction of capillary pressure versus non-wetting phase saturation for the DM samples SGL 24BC (5 wt.% of PTFE) and SGL 24DC (20 wt.% of PTFE) under no compression. Recalling that the benchmark data were generated for the DM samples coated with micro-porous layer, the nature of the capillary pressure–saturation curves shown in Fig. 3 exhibits a continuous "S" shape, indicating the highly non-linear relationship between the capillary pressure and the saturation of the tested bi-layered DM samples. The ANN predictions appear to successfully follow the complex shape of the measured capillary pressure within an average uncertainty of ±5.1% of the measured data over the entire saturation

domain ($0 < s_{nw} < 1$). This indicates that the designed network can accurately capture the corresponding change in the measured capillary pressures in response to the increase in PTFE content of the DM. The comparison was also performed for the tested DM samples under different compressions. Fig. 3b represents the comparison of measured capillary pressure and the ANN prediction for SGL 24BC (20 wt.% of PTFE) DM exposed to 0 and 1.4 MPa compression (two measurement boundaries). The present ANN model successfully performs the necessary adjustments to predict the capillary pressure in response to the change in compression, thereby precisely capturing the measured capillary pressures within an average uncertainty of ±4.8% of the measured data in the entire saturation range, even in the high capillary pressure zone ($s_{nw} > 0.7$) which is governed by the hydrophobic micro-porous layer [3–5] (Fig. 3b).

2.4. Empirical correlation and ANN implementation

Recently, our group has published three papers [6–8] that are devoted to developing a validated capillary pressure–saturation relationship (for drainage in hydrophobic pores) appropriate for the tested fuel cell DM materials. The unified capillary pressure–saturation correlation presented in the final part of this paper series [8] was deduced from the same extensive benchmark data that has also been used in this study to train the designed artificial neural network. In our previous study [8], a multi-dimensional linear regression model was employed to determine the best polynomial fit that correlates the capillary pressure with the relevant non-dimensionalized experimental parameters. In order to improve the precision of the empirical correlation and eliminate the potential uncertainty associated with the complex shape of the capillary pressure–saturation curves, the overall saturation domain was divided into three regions. The characteristic capillary pressure–saturation equation derived for these tested DM samples was suggested as follows [8]:

$$P_C = \underbrace{(293/T)^6 \gamma(T)}_{\text{Temperature effect}} \underbrace{2^{0.4C}\sqrt{\frac{\varepsilon_c}{k}}}_{\text{Compression effect}} \underbrace{K(S_{nw})}_{\text{Mixed wettability}} \quad (1)$$

$$K(s) = \begin{cases} (\text{wt.\%})\left[0.0469 - 0.00152(\text{wt.\%}) - 0.0406 s_{nw}^2 + 0.143 s_{nw}^3\right] + 0.0561 \ln s_{nw} & 0 < s_{nw} \le 0.50 \\ (\text{wt.\%})\left[1.534 - 0.0293(\text{wt.\%}) - 12.68 s_{nw}^2 + 18.824 s_{nw}^3\right] + 3.416 \ln s_{nw} & 0.50 < s_{nw} \le 0.65 \\ (\text{wt.\%})\left[1.7 - 0.0324(\text{wt.\%}) - 14.1 s_{nw}^2 + 20.9 s_{nw}^3\right] + 3.79 \ln s_{nw} & 0.65 < s_{nw} < 1.00 \end{cases}$$

where C, ε_c, k, and γ represent the compression pressure, compressed porosity, absolute permeability and surface tension. The parameters in $K(s_{nw})$ namely; (wt.%) and s_{nw} are PTFE weight percentage and non-wetting liquid saturation, respectively. Note that the porous media of interest herein is a composite structure. The capillary pressure–saturation curves of the DM macro-substrate (without MPL) can be extracted from the overall behavior of the composite structure by using the corresponding the pore size distribution and porosities of the macro- and micro-substrate (MPL), as also discussed in Refs. [6–8,29].

As shown in Eq. (1), the given empirical correlation is highly non-linear, introducing additional complexity when used in an advanced computational model. As also noted in the introduction section, existing fuel cell models [33,34] are already computationally complex, and somewhat limited by assumptions and correlations. Moreover, these models are mostly constructed by isolating a certain physical mechanism from the overall complex transport scheme to avoid additional mathematical complexity. There is still too much uncertainty involved to achieve the goal of a completely predictive whole-cell multi-phase transient model. In addition, when the design and optimization are considered from a manufacturer's perspective, there are other parameters such as material properties, application type, binder and fiber type, labor and manufacturing cost that need to be accounted for in the computational framework. However, identifying the relevant physical connections between these manufacturing variables and the other relevant transport properties is extremely difficult, and complicates the task of designing such a tool based on a conventional CFD model.

As such, this study is devoted to introducing an alternative approach based on artificial neural network that can effectively correlate all these complex variable in one domain in the absence of physical connections [27,28]. As a first step of development of such a design tool, we have analyzed the effectiveness of

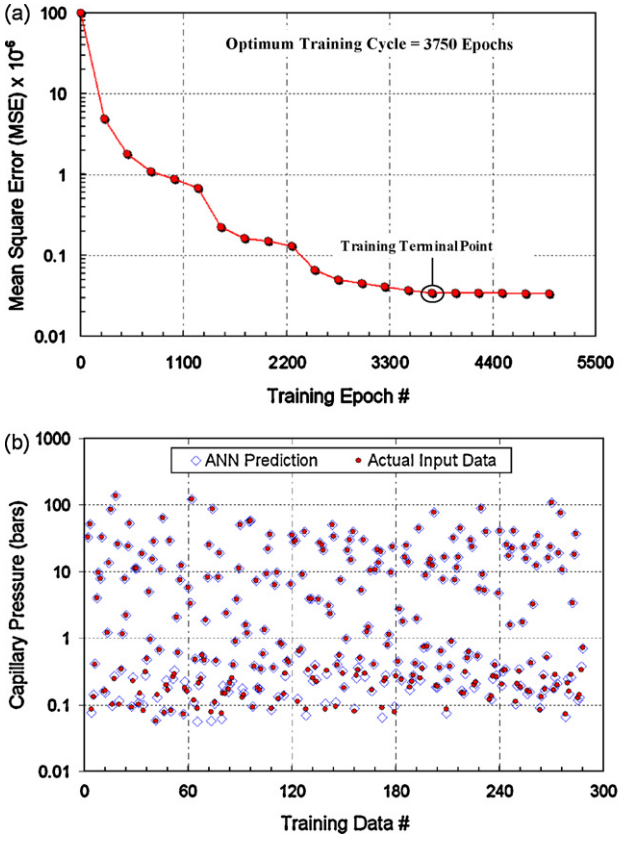

Fig. 2. (a) Training epoch cycles vs. calculated mean square error of the supervised training for the designed ANN and (b) comparison of actual input data and corresponding ANN predictions for the training data set.

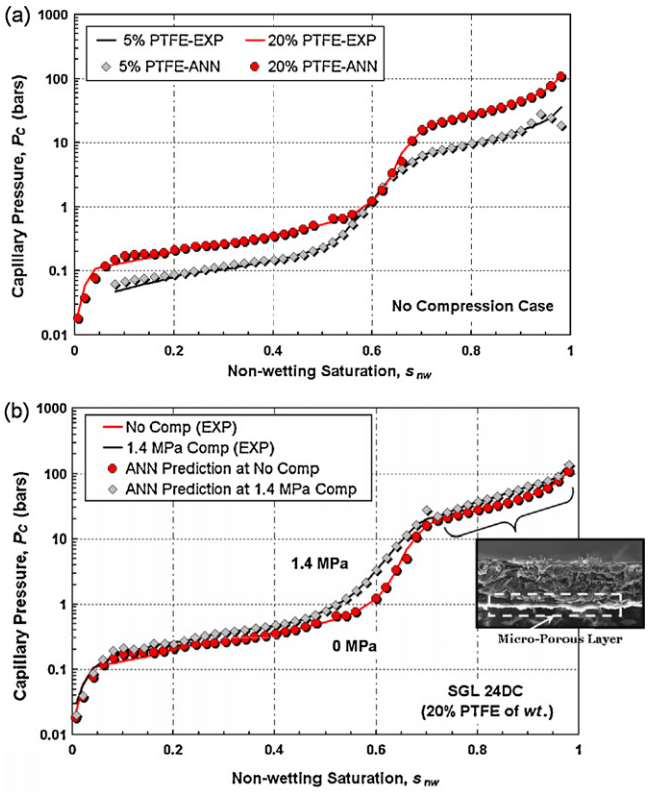

Fig. 3. Comparison of experimental data [6–8] and ANN predictions for: (a) SGL 24BC (5% PTFE) and SGL 24DC (20% PTFE) under no compression and (b) SGL 24DC (20% PTFE) under no compression and 1.4 MPa compression.

implementation of ANN to characterize the capillary transport of the fuel cell DM.

3. Results and discussions

The well-known limitation of the ANN system is its insufficient capability of performing extrapolations [27,28]. Since the learning mechanism is achieved by training the network with the specified data set, the neural network can only represent the characteristic patterns of the given data points. When the data point of interest is beyond the range of original training data set, the response (prediction) of the trained network exhibits unpredictable performance, yielding significantly low accuracy. In order to minimize the impact of this limitation, the benchmarking experiments [6–8] have been performed at well-designed test conditions, which cover the typical hydrophobic treatment range of the fuel cell DM (5–20 wt.% of PTFE) and the assembly compression pressure range (0–1.4 MPa) typically encountered in fuel cell applications. Therefore, recalling that the experiments described herein were performed at 0, 0.6 and 1.4 MPa for the DM samples treated with different PTFE content (5, 10 and 20 wt.%), in the present study, the main effort is focused on evaluating the relative significance of PTFE content and compression of the DM on the capillary pressure at the intermediate testing conditions within the range of tested parameters (*i.e.*, 5% < PTFE < 20% and 0 < C < 1.4 MPa), in which the experimental data are not available.

3.1. Degree of mixed wettability

The degree of PTFE loading in DM plays a deterministic role in the capillary transport mechanism, since any increase in PTFE loading facilities the water removal rate from the pores, therefore leading to a considerable reduction in the water retention (water storage) capacity of the DM. In order to elucidate the relative significance of PTFE content, the designed ANN was simulated to predict the capillary pressure as a function of PTFE loading of the DM at different saturations. Fig. 4 shows the predicted capillary pressure versus % PTFE content of the DM at different saturations (*i.e.*, 0.1, 0.2, 0.3 and 0.4) under two different compressions, namely 0.3 MPa and 0.9 MPa (*i.e.*, the intermediate conditions for which the experimental data are not available). As seen in both Fig. 4a and b, the predicted capillary pressure follows an increasing trend with an increase in PTFE content for all saturations, however it exhibits relatively higher increase for high saturations (*i.e.*, s_{nw} = 0.3 and 0.4). In other words, the sensitivity of the capillary pressure on the hydrophobicity

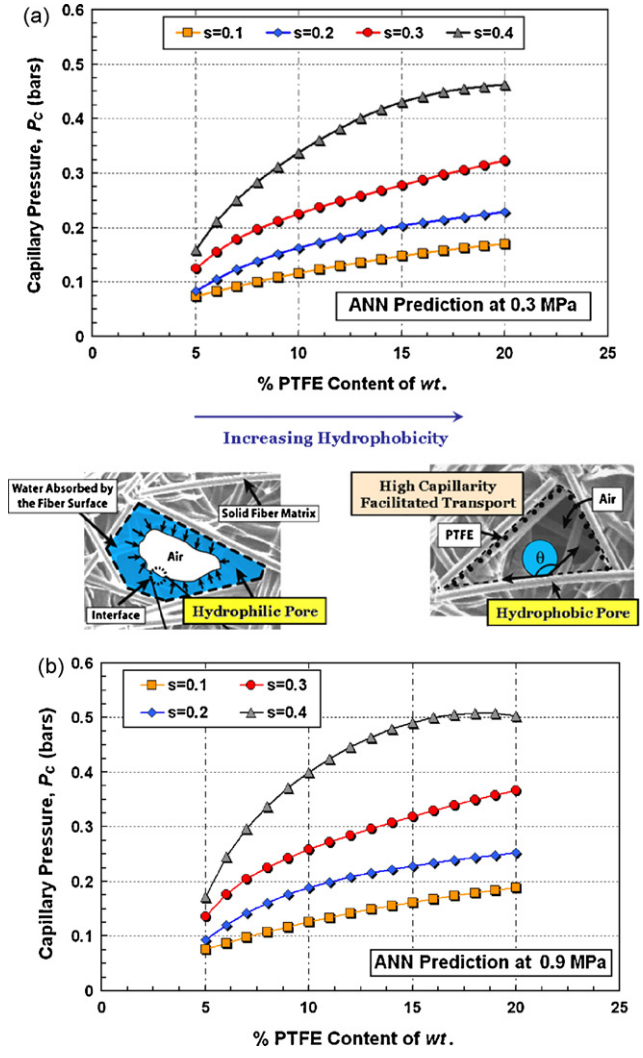

Fig. 4. ANN prediction of capillary pressure vs. % PTFE content of DM at different saturations: (a) under 0.3 MPa compression and (b) under 0.9 MPa compression.

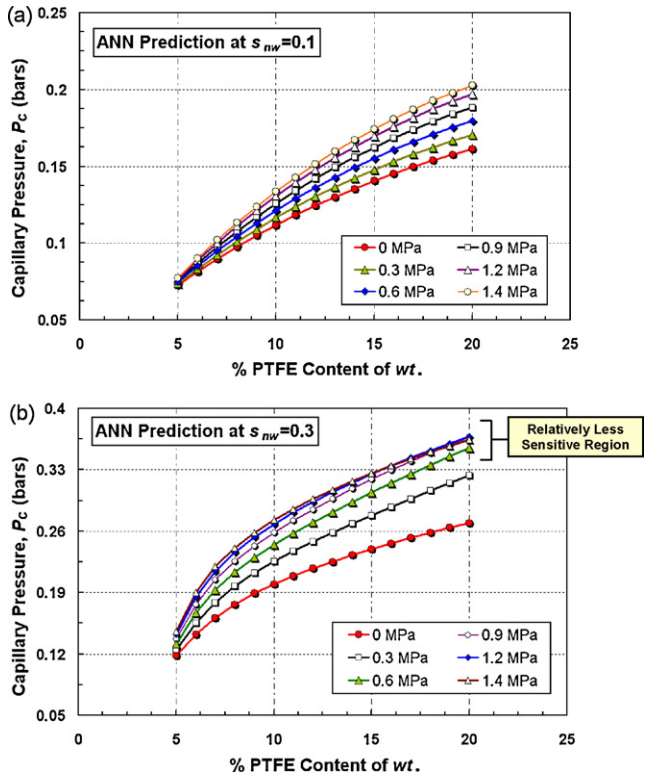

Fig. 5. ANN prediction of capillary pressure vs. % PTFE content of DM under different compressions (intermediate conditions for which the experimental data are not available) at a constant saturation of: (a) 0.1 and (b) 0.3.

appears to increase with saturation, in a good agreement with the experimental observations presented in Refs. [6–8]. This can be attributed to the strong dependence of capillary pressure on the local water content of the pore and the hydrophobicity of the pore matrix. Physically, at pore level, any increase in the liquid saturation leads to an increase in the liquid pressure, which is directly proportional to the capillary pressure. In addition, rendering the pore surface more hydrophobic distorts the molecular force balance at the line of contact, forcing the liquid water to move towards an unstable state, which in turn, leads to a higher capillary pressure within the pore.

3.2. Compression loading

The designed ANN algorithm was utilized to delineate the response of the capillary pressure to any change in the compression pressure applied on the DM. Fig. 5 shows the predicted capillary pressure versus % PTFE content of the DM at constant saturations ($s_{nw} = 0.1$ and $s_{nw} = 0.3$) under different compression conditions ranging from 0 to 1.4 MPa with an increment of 0.3 MPa (*i.e.*, the intermediate conditions for which the experimental data are not available). The ANN simulations reveal that for a given PTFE loading, the capillary pressure is prone to increase in parallel with an increase in compression. The increase in capillary pressure with compression can be attributed to the corresponding reduction in pore size, which can be explained through the Young–Laplace theorem. The Young–Laplace theorem (Eq. (2)) correlates the capillary pressure for a cylindrical pore in terms of pore radius, surface tension and contact angle:

$$P_C = \frac{2\gamma \cos\theta}{r} \tag{2}$$

where P_C, γ, θ and r represent the capillary pressure, surface tension, contact angle and pore radius, respectively. Based on the theoretical description given in Eq. (2), applying compression on the DM reduces the available pore volume and consequently decreases the pore radius, therefore leading to a higher capillary pressure.

One other observation that can be drawn from Fig. 5 is that the increase in capillary pressure with compression exhibits dissimilar behaviors in different compression ranges for different saturation cases. For the low saturation case ($s_{nw} = 0.1$) as shown in Fig. 5a, the capillary pressure appears to increase almost linearly with compression (diminishing importance) for any specified PTFE content within the simulated compression range (from 0 to 1.4 MPa). However, for the higher saturation case ($s_{nw} = 0.3$), the increase in capillary pressure with compression is more pronounced between an uncompressed and 0.6 MPa compression condition, especially for DMs having % PTFE content higher than 10%. Any further increase in compression pressure from 0.6 to 1.4 MPa seems to have relatively less effect on the predicted capillary pressure (Fig. 5b), which is in good agreement with our previous experimental observations [6–8].

As shown in Fig. 5b, for the DM coated with 15% PTFE, the predicted capillary pressure exhibits a 26% increase with an increase in compression from 0 to 0.6 MPa, whereas a 7% increase of the capillary pressure is predicted as the compression is further increased from 0.6 to 1.4 MPa. This behavior can be linked to the relatively higher spread out of the hydrophilic sites compared to the hydrophobic ones within this compression range. Any further increase in compression from 0.6 MPa seems to promote the dispersion of more hydrophilic sites, producing higher hydrophilic surface area. As a result, the expansion of the hydrophilic sites with compression enhances the hydrophilic characteristic of the DM, impeding the increase in capillary pressure within the pore matrix, which is in good agreement with the observations reported by Bazylak et al. [16].

3.3. PTFE and compression: coupled effect

As described in previous sections, both PTFE loading of the DM and compression have strong influences on the capillary pressure. However, the engineering consequences of increasing PTFE content and compression should be systematically optimized in order to minimize the additional losses introduced by these parameters. For that purpose, the relative significance of these parameters on the capillary transport characteristics of the DM was investigated. The present neural network was utilized to determine the capillary pressure as a function of PTFE loading and compression pressure. Fig. 6 depicts the capillary pressure predictions of the ANN simulations as a function of compression pressure at different PTFE loadings for a specified saturation ($s_{nw} = 0.3$). As seen from Fig. 6, the effect of com-

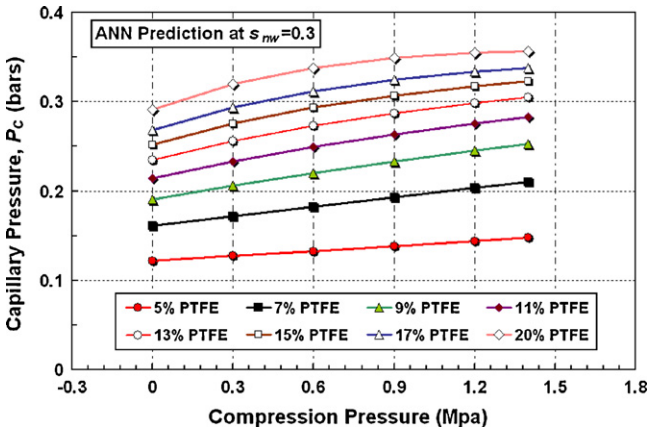

Fig. 6. ANN prediction of capillary pressure vs. compression pressure of DMs treated with different PTFE loadings at constant saturation of 0.3.

pression on the capillary pressure is observed to be amplified with an increase in PTFE loading of the DM. This suggests that from capillary transport perspective, tailoring the DM with higher PTFE loading and applying high compression would lead to a higher capillary pressure at a given saturation, therefore promoting the liquid water transport within the pores of the DM. However, in terms of system efficiency, increasing PTFE loading of the DM would introduce an additional electrical loss, and applying high compression may cause permanent deformation, therefore facilitating the degradation mechanism, which is not desirable in terms of longevity and durability.

4. Conclusions

An artificial neural network was designed and trained with the benchmark data generated from the capillary pressure–saturation measurements [3–5] of SGL 24 series carbon paper DMs treated with different PTFE undergoing various compression loadings. The detailed comparison of the ANN predictions with the experimental data was performed. The results confirm that ANN predictions are consistent with those obtained from experimental analysis [6–8], yielding an average uncertainty of ±5.1% of the measured data. After performing validation, the present neural network algorithm was utilized to predict the response of the change in capillary pressure of the DM as a function of PTFE loading and compression at intermediate conditions, where the experimental data are not available.

The ANN simulations show that the capillary pressure is prone to increase in parallel with the PTFE loading of the DM and the applied compression pressure, especially within the compression range of 0–0.6 MPa. Any further increase in compression above 0.6 MPa appears to have relatively less impact on the capillary pressure due to the relatively higher dispersion of the hydrophilic sites within the compression range from 0.6 to 1.4 MPa. Furthermore, any increase in hydrophobicity of the DM is found to amplify the compression effect, yielding a higher capillary pressure, possibly because of the reduction in effective pore size and enhanced molecular imbalance at the phase interface.

The artificial intelligence model presented herein can be further extended into a more detailed design algorithm that couples the DM internal architecture with the cell performance, manufacturer variables and operating conditions as more benchmark data are available. Such a tool can potentially reduce the number of experiments required and provide improved means of selecting the optimum electrode configurations suitable for different fuel cell operations. Our team is rapidly expanding the existing database. The development of an advanced design tool based on this framework is ongoing work in our laboratory and will be reported in subsequent publications.

Acknowledgments

This research is partially supported by NSF grant no. CTS-0414319. Dr. E.C. Kumbur would like to thank Mr. Basar Basbug and Mr. Emre Artun for their assistance during preparation of this manuscript.

References

[1] E.C. Kumbur, K.V. Sharp, M.M. Mench, J. Power Sources 168 (2007) 356.
[2] A. Kraytsberg, Y. Ein-Eli, J. Power Sources 160 (2006) 194.
[3] S. Escribano, J.-F. Blachot, J. Etheve, A. Morin, R. Mosdale, J. Power Sources 156 (2006) 8.
[4] W. He Lin, T. Van Nguyen, J. Electrochem. Soc. 151 (2004) A1999.
[5] H.-K. Lee, J.-H. Park, D.-Y. Kim, T.-H. Lee, J. Power Sources 131 (2004) 200.
[6] E.C. Kumbur, K.V. Sharp, M.M. Mench, J. Electrochem. Soc. 154 (12) (2007) B1295–B1304.
[7] E.C. Kumbur, K.V. Sharp, M.M. Mench, J. Electrochem. Soc. 154 (12) (2007) B1305–B1314.
[8] E.C. Kumbur, K.V. Sharp, M.M. Mench, J. Electrochem. Soc. 154 (12) (2007) B1315–B1324.
[9] V. Gurau, M.J. Bluemle, E.S. De Castro, Y.-M. Tsou, J.A. Mann, T.A. Zawodzinski Jr., J. Power Sources 160 (2006) 1156.
[10] J. Divisek, J. Fuhrmann, K. Gartner, R. Jung, J. Electrochem. Soc. 150 (2003) A811.
[11] G. Hea, P. Mingb, Z. Zhaoa, A. Abudulac, Y. Xiaob, J. Power Sources 163 (2007) 864.
[12] J.T. Gostick, M.A. Ioannidis, M.W. Fowler, M.D. Pritzker, J. Power Sources 173 (2007) 277.
[13] J.H. Nam, M. Kaviany, Int. J. Heat Mass Transf. 46 (2003) 4595.
[14] J. Ge, A. Higier, H. Liu, J. Power Sources 159 (2006) 922.
[15] I. Nitta, T. Hottinen, O. Himanen, M. Mikkola, J. Power Sources 171 (2007) 26.
[16] A. Bazylak, D. Sinton, Z.-S. Liu, N. Djilali, J. Power Sources 163 (2007) 784–792.
[17] V.P. Schulz, J. Becker, A. Wiegmann, P.P. Mukherjee, C.Y. Wang, J. Electrochem. Soc. 154 (2007) B419.
[18] N. Djilali, Energy 32 (2007) 269.
[19] S.A. Kalogirou, Renew. Sust. Energy Rev. 5 (2001) 373.
[20] S. Qu, L.E.K. Achenie, J. Power Sources 140 (2003) 319.
[21] E. Entchev, L. Yang, J. Power Sources 170 (2007) 122.
[22] I. Arriagada, P. Olausson, A. Selimovic, J. Power Sources 112 (2002) 54.
[23] W.-Y. Lee, G.-G. Park, T.-H. Yang, Y.-G. Yoon, C.-S. Kim, Int. J. Hydrogen Energy 29 (2004) 961.
[24] L.C. Kiong, M. Rajeswari, M.V.C. Rao, Appl. Soft Comput. 3 (2003) 159–175.
[25] S.O.T. Ogaji, R. Singh, P. Pilidis, M. Diacakis, J. Power Sources 154 (2006) 192.
[26] A. Saengrung, A. Abtahi, A. Zilouchian, J. Power Sources 172 (2007) 749.

[27] S. Haykin, J. Math. Psychol. 41 (1997) 287.
[28] H. El Kadi, Compos. Struct. 73 (2006) 1.
[29] J.T. Gostick, M.W. Fowler, M.A. Ioannidis, M.D. Pritzker, Y.M. Volfkovich, A. Sakars, J. Power Sources 156 (2006) 375.
[30] M. Acosta, C. Merten, G. Eigenberger, H. Class, R. Helmig, B. Thoben, H. Muller-Steinhagen, J. Power Sources 159 (2006) 1123.
[31] J.D. Fairweather, P. Cheung, J. St-Pierre, D.T. Schwartz, Electrochem. Commun. 9 (2007) 2340.
[32] Y.M. Volfkovich, V.S. Bagotzky, V.E. Sosenkin, I.A. Blinov, Colloids Surf. A: Physicochem. Eng. Aspects 187-188 (2001) 349.
[33] C.Y. Wang, Chem. Rev. 104 (2004) 4727.
[34] D. Cheddie, N. Munroe, J. Power Sources 147 (2005) 72.